Earth's Future

RESEARCH ARTICLE
10.1029/2019EF001393

Greenland Ice Sheet Response to Stratospheric Aerosol Injection Geoengineering

John C. Moore[1,2,3], Chao Yue[1], Liyun Zhao[1,4], Xiaoran Guo[1], Shingo Watanabe[5], and Duoying Ji[1]

[1]College of Global Change and Earth System Science, Beijing Normal University, Beijing, China, [2]Arctic Centre, University of Lapland, Rovaniemi, Finland, [3]CAS Center for Excellence in Tibetan Plateau Earth Sciences, Beijing, China, [4]Southern Marine Science and Engineering Guangdong Laboratory (Zhuhai), Zhuhai, China, [5]Japan Agency for Marine-Earth Science and Technology, Yokohama, Japan

Key Points:
- We examine the impact of stratospheric aerosol geoengineering on both the surface ice sheet water runoff and the dynamic loss of ice
- Aerosol injection of ¼ 1991 Pinatubo volcanic eruption per year slows mass loss by 15–20% mainly due to reduced surface melting
- Increased Arctic sea ice and reduced humidity cool the ablation zone sufficiently to overcome a slightly increased AMOC relative to RCP4.5

Supporting Information:
- Supporting Information S1

Correspondence to:
L. Zhao,
zhaoliyun@bnu.edu.cn

Citation:
Moore, J. C., Yue, C., Zhao, L., Guo, X., Watanabe, S., & Ji, D. (2019). Greenland ice sheet response to stratospheric aerosol injection geoengineering. *Earth's Future*, *7*, 1451–1463. https://doi.org/10.1029/2019EF001393

Received 18 OCT 2019
Accepted 11 DEC 2019
Accepted article online 14 DEC 2019
Published online 29 DEC 2019

Author Contributions:
Conceptualization: John C. Moore
Data curation: Chao Yue
Formal analysis: John C. Moore, Chao Yue, Liyun Zhao, Xiaoran Guo, Shingo Watanabe, Duoying Ji
Funding acquisition: John C. Moore
Investigation: John C. Moore, Chao Yue, Xiaoran Guo, Shingo Watanabe, Duoying Ji
Methodology: John C. Moore
Project administration: John C. Moore
Resources: John C. Moore
(continued)

Abstract The Greenland ice sheet is expected lose at least 90% of its current volume if ice sheet summer temperatures warm by around 1.8 °C above pre-industrial. Geoengineering by stratospheric sulfate aerosol injection might slow Greenland ice sheet melting and sea level rise by reducing summer temperature and insolation; however, such schemes could also reduce precipitation and affect large-scale climate drivers such as the Atlantic Meridional Over-turning Circulation (AMOC). Earlier work found that AMOC increased under geoengineering and that might lead to greater mass loss from Greenland than under greenhouse gas forcing alone. We simulated Greenland ice sheet climates using four Earth system models running the stratospheric sulfate aerosol injection experiment GeoMIP G4 and the CMIP RCP4.5 and RCP8.5 greenhouse gas scenarios that were then used to drive the surface energy and mass balance model, SEMIC. Simulated runoff is 20% lower under G4 than RCP4.5, while under RCP8.5 it is 17% higher. The mechanism is through increased Arctic sea ice concentration and reduced humidity leading to surface cooling of the ablation zone. Reduced absorption of outgoing longwave radiation caused by hydrological cycle weakening dominates associated decreases in precipitation under geoengineering and stronger AMOC than under RCP4.5. An ice dynamics model simulates 15% lower ice losses under G4 than RCP4.5. Thus, total sea level rise by 2070 from the Greenland ice sheet under G4 geoengineering is about 15–20% lower than under the RCP4.5 scenario.

Plain Language Summary Mass loss from the Greenland ice sheet is expected to raise sea levels by tens of centimeters this century and far more in the further future. Rising seas are one of the most damaging aspects of the warming climate, affecting hundreds of millions, and costing $ trillions by 2100, and geoengineering might be one approach that could be used against this threat. But the North Atlantic climate is a complex region where the flux of warm tropical waters is being reduced by greenhouse warming, which geoengineering would reverse. Hence, how Greenland would likely respond is a key factor in deciding the potential utility of doing geoengineering. We examine the impact of stratospheric aerosol geoengineering on both the surface ice sheet water runoff (which accounts for half of present-day ice loss) and the dynamic loss of ice from fast-flowing glaciers that are being accelerated by warming ocean currents (accounting for the other half). We find that aerosol injection equivalent to about ¼ Pinatubo volcanic eruption per year can slow mass loss from Greenland by 15–20% compared with greenhouse gas forcing alone, mainly due to reduced surface melting.

1. Introduction

As temperatures have risen over the last few decades, the Greenland ice sheet's surface mass balance (SMB) has become increasingly more negative (Hanna et al., 2013; Rignot et al., 2008). Projections of Greenland's future contributions to sea level rise are about 10–20 cm by the year 2100 (Jevrejeva et al., 2016), with about half this amount coming from surface runoff, and the other half from iceberg calving along the marine margins of the ice sheet (van den Broeke et al., 2009). In the longer term, the Greenland ice sheet is expected lose at least 90% of its current volume if ice sheet summer temperatures warm by around 1.8 °C above pre-industrial (Pattyn et al., 2018). Mass loss from the ice sheet may also impact the Atlantic thermohaline circulation by changing the density structure of the ocean near the overturning points, and Arctic sea ice cover, both of which have implications ranging from impacts on indigenous lifestyles to global climate change.

Software: John C. Moore, Chao Yue, Xiaoran Guo
Supervision: John C. Moore, Liyun Zhao
Validation: Chao Yue, Liyun Zhao
Writing - original draft: Chao Yue
Writing – review & editing: John C. Moore, Liyun Zhao, Xiaoran Guo, Duoying Ji

Geoengineering has been proposed as a way to limit global warming by deliberately altering the climate to both alleviate some of the consequences of anthropogenic greenhouse gas emissions (Irvine et al., 2018) and as part of strategic approach to keep temperatures below thresholds such as 1.5 °C above pre-industrial (Jones et al., 2018; MacMartin & Kravitz, 2019). Climate models simulating the Atlantic Meridional Overturning Circulation (AMOC) show that it decreases in intensity as atmospheric greenhouse gas concentrations and temperatures rise. Geoengineering that reduces surface temperature rises restores the AMOC to levels close to but still lower than present-day levels (Hong et al., 2017). However, recent simulations with one climate model (Fasullo et al., 2018) showed AMOC to be over-compensated when temperatures were stabilized at present-day levels, and hence, Greenland could actually suffer relatively more ice loss than without geoengineering.

Stratospheric aerosol injection (SAI) with sulfate aerosols is the most commonly simulated geoengineering proposal. Earth system model (ESM) simulations confirm expectations from physical principles, that climate system thermodynamics will change when a reduction in shortwave (SW) radiative flux is designed to offset increases in longwave (LW) absorption from greenhouse gases (Huneeus et al., 2014). Since greenhouse gases absorb radiation within the atmosphere continuously, while incoming solar radiation mostly heats the surface during the day, the spatial and temporal patterns of LW and SW forcing will vary depending on how it is done; for example, with injections into the equatorial lower stratospheric, the tropics are cooled relatively more than the polar regions (e.g., Kravitz et al., 2013). These spatial and seasonal differences in radiative forcing patterns lead to changes in large-scale circulation systems such as the AMOC (Fasullo et al., 2018; Hong et al., 2017) and teleconnection patterns (Moore et al., 2014). It is this systematic bias in spatial temperatures under equatorial SAI that led to simulations aimed at maintaining existing equator to pole temperature gradients by specifying aerosol injection at latitudes up to 30° (Tilmes et al., 2018).

The few Greenland studies considering SAI geoengineering simulated by single ESM note nonlinearities (Irvine et al., 2010) and hysteresis (Applegate & Keller, 2015) in the long-term ice sheet response, so that restoring temperatures may not lead to a recovery of the ice sheet. But solar geoengineering could slow ice melting compared with greenhouse forcing alone, and in multi-model simulations of the glaciers in High Mountain Asia, this amounted to about a 30% reduction in sea level commitment by 2070 (Zhao et al., 2017). These studies used simplified surface mass and energy balance parameterizations, often forced by changes in temperature and precipitation only. However, ignoring changes in downward radiation flux may underestimate the effectiveness of solar geoengineering at offsetting melt in Greenland (Irvine et al., 2018). SW radiation accounted for nearly half of the change in SMB during the Eemian period (Van de Berg et al., 2011), with only about half due to ambient temperature. The substantial reduction in cloud cover over Greenland during the past two decades has altered the surface radiation balance and is the likeliest cause for recent acceleration in mass loss from the ice sheet (Hofer et al., 2017).

2. Methods

2.1. Climate Models and Scenarios

We estimate ice sheet SMB and the dynamic response of the fastest glacier and largest contributor to sea level rise in Greenland under climate projections from four ESMs (Table 1) driven by the IPCC RCP4.5, RCP8.5 (Taylor et al., 2012), and Geoengineering Model Intercomparison project (GeoMIP; Kravitz et al., 2011) G4 scenarios. We look at the 50-year period of SAI, 2020–2069, and the 20 years following its termination, 2070–2089. The G4 scenario is based on the RCP4.5 greenhouse gas scenario, with the addition of SO_2 injected into the equatorial lower stratosphere at a rate of 5 Tg year^{-1} corresponding to about ¼ of the amount injected by the 1991 eruption of Mt. Pinatobo (Bluth et al., 1992).

We focus on RCP4.5 and G4 as the most policy relevant scenarios since the Intended Nationally Determined Contributions greenhouse gas emissions framework would produce temperature trajectories similar to RCP4.5 (Kitous & Keramidas, 2015); the stratospheric sulfate loading required under G4 is more plausible than, for example, the 10 times larger injection rates (Fasullo et al., 2018; Tilmes et al., 2018) needed to offset RCP8.5 at the end of the century. We wish to explore quantitatively how Greenland's SMB responds to SAI combined with greenhouse gas forcing and how the regional changes in circulation and hydrological cycle interact with local changes to modify glacier dynamics. Since each ESM represents and parameterizes various physical processes in particular ways, they produce quite different emergent features such as AMOC

Table 1
Models Used in This Study

Model	Resol'n runs	Snowmelt scheme	Snow layers	Snow/ice albedo	Density	Runoff method
BNU-ESM[a]	2.8° × 2.8° 1	Common land Model CoLM[d]	Dynamic (max. 5)	Age, grain size, solar zenith angle, fresh snow	Snow depth, compaction	Bucket-type following TOPMODEL[e]
MIROC-ESM[b]	2.8° × 2.8° 1	MATSIRO[f]	Dynamic (max. 3)	Prognosticated from snow temperature and age	Fixed 300 kg m^{-3}	Bucket-type following TOPMODEL[e]
†MIROC-ESM-CHEM[b]	2.8° × 2.8° 3					
HadGEM2-ES[c]	1.25° × 1.875° 3	Surface energy and mass balance	Single	Prescribed deep snow values with masking by snow depth	Fixed 250 kg m^{-3}	TOPMODEL[e]
SEMIC[g]	0.5° × 0.5° 8 × Σruns	Surface energy and mass balance model	Single	8 types (Text S1)	Snow depth	Ice melt
Positive degree day (PDD[h])	0.5° × 0.5° 1 × Σruns	Linear with surface temperature	—	—	—	Ice melt

Note. Each ESM was weighted equally in the ensemble regardless of number of runs per model. MIROC-ESM-CHEM shares the same snowmelt and runoff model as MIROC-ESM.
[a]Ji et al. (2014). [b]Watanabe et al. (2011). [c]Collins et al. (2011). [d]Dai et al. (2003). [e]Beven and Kirby (1979). [f]Takata et al. (2003). [g]Braithwaite (1995). [h]Krapp et al. (2017).

or teleconnection patterns. Using a multi-model ensemble provides a way of estimating across-model uncertainty in the response of a particular system—in this case the Greenland ice sheet that would not be available from an ensemble of any single model, no matter if that model possesses certain very advanced features, such as excellent stratospheric chemistry and physics.

We use all ESMs that have daily mean values of incoming SW and LW radiation, near-surface air temperature, surface wind speed, near-surface specific humidity, surface pressure, snowfall, and rainfall available for G4, RCP4.5, and RCP8.5 as well as the historical period. MIROC-ESM and MIROC-ESM-CHEM share many of the same model components, and we tested the effects of de-weighting them relative to the other models but find that it makes little difference to results; for example, 0.75 weights in the ensemble changes mean SMB by <2%.

2.2. Downscaling

As the climate models have relatively coarse resolution (Table 1), we downscale them to better capture the ablation areas around the margins of the ice sheet. The four-ESM temperature fields were statistically downscaled to 0.5° × 0.5° using an altitude temperature lapse rate of 0.65 °C (100 m)$^{-1}$. Incoming SW and LW radiation, surface wind speed, near-surface specific humidity, surface pressure, snowfall, and rainfall are bilinearly interpolated into the same 0.5° × 0.5° grid. Because the correlation between precipitation and elevation is small and highly heterogeneous (Noël et al., 2016), we did not correct the precipitation for elevation using a precipitation lapse rate. We bias corrected the downscaled daily data with Inter-Sectoral Impact Model Intercomparison Project (ISI-MIP; Hempel et al., 2013) methods using 0.5° × 0.5° ERA-Interim (Simmons, 2006) from 1979 to 2004 as the observation-based reference climate (Figure 1). ESM temperature and precipitation fields, which we shall show are the main drivers of SMB changes, are well correlated with ERA-Interim reanalysis products spatially over Greenland. Observed precipitation tends to underestimate snowfall under windy conditions leading to differences with estimates from the regional climate model RACMO driven from ERA-40 (Ettema, 2009), but applying a standard correction to snowfall (Yang et al., 2005) offsets this effect and yields correlations of 0.9 with 20 manned stations. Our analysis of the ESM products we use and data from seven stations around the Greenland margin finds similar results and correlations of 0.87.

2.3. SEMIC

SEMIC is a physically based model utilizing an energy balance approach that can quickly compute SMB, runoff, and snow pack properties due to its one-layer snowpack and relatively modest data input requirement. SEMIC simulates future changes in surface temperature and SMB (Krapp et al., 2017) in good agreement with the more sophisticated multilayer snowpack model SISVAT included in the regional climate

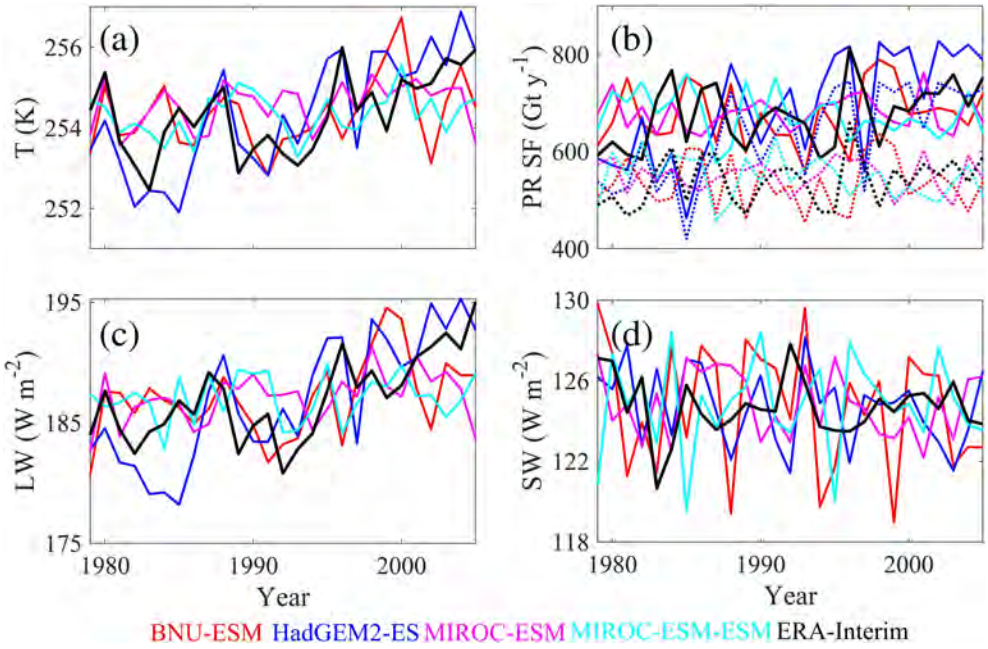

Figure 1. Historical time series of (a) annual bias-corrected near-surface air temperature, (b) precipitation (solid) and snowfall (dashed), (c) downward longwave radiation, and (d) downward shortwave radiation during 1979–2005 by BNU-ESM (red), HadGEM2-ES (blue), MIROC-ESM (magenta), MIROC-ESM-CHEM (cyan), and ERA-Interim (black) over Greenland.

model, MAR (Fettweis et al., 2013). We use the same values for all free parameters in SEMIC as Krapp et al. (2017). Surface melt causes the positive melt-albedo feedback which results in lower albedo in high-melt years (Stroeve, 2001). Hence, modeled SMB is highly sensitive to albedo parameterizations. Surface albedo is the average of snow albedo and the background albedo, and we consider two surface albedo and four snow albedo parameterizations, making eight in total (supporting information, Text S1). Comparison between MAR forced by ERA-Interim and SEMIC forced by downscaled output from the four ESMs (Figure 2) shows that the envelope of albedo parameterizations encloses the MAR results, but no particular choice is better than the others, hence keeping all eight allows a reasonable estimate of uncertainty.

In addition to SEMIC, we also used a simple positive degree day PDD scheme and the ESM runoff output (Text S1 and Table 1). All three methods were tested with historical simulation data and verified by comparison with the state-of-the-art regional SMB model, MAR (Fettweis et al., 2013) driven by ERA-Interim (Simmons, 2006) with ½° spatial and 6-hourly resolutions from 1979 to 2004 (Figure S1). The PDD scheme clearly underestimates runoff, while the SEMIC and ESM outputs are quite consistent with the best available estimates during the historical period (Figure S1), although SEMIC produces more runoff than ESM estimates. The similarity of the ESM results to best estimates in the historical period is slightly surprising given the relatively coarse model resolutions, but this also suggests that the ½° resolution SEMIC simulations are fine enough to capture important topographic effects.

2.4. Correction of SEMIC Modeled SMB Due to SMB-Elevation Feedback

We considered the impact of changing surface topography over the 21st century—increased ablation at the ice margin will lower it, increasing its temperature leading to further increased melt. We divided the ice sheet into three regions and analyzed the correlation between SMB and surface elevation, in accumulation zone and ablation zone, respectively, in each subregion over the historical period 1979–2005. Surface elevation data (Morlighem et al., 2017) were from the period of 1993–2016, and we assumed it represented that in 1979–2005. We found the only significant ($P < 0.01$) correlation in ablation zone of the South-Western region, and this was consistent for all four ESMs. Therefore, we only applied a SMB correction to the South-Western ablation region. We assumed steady state for the historical period 1979–2005; that is,

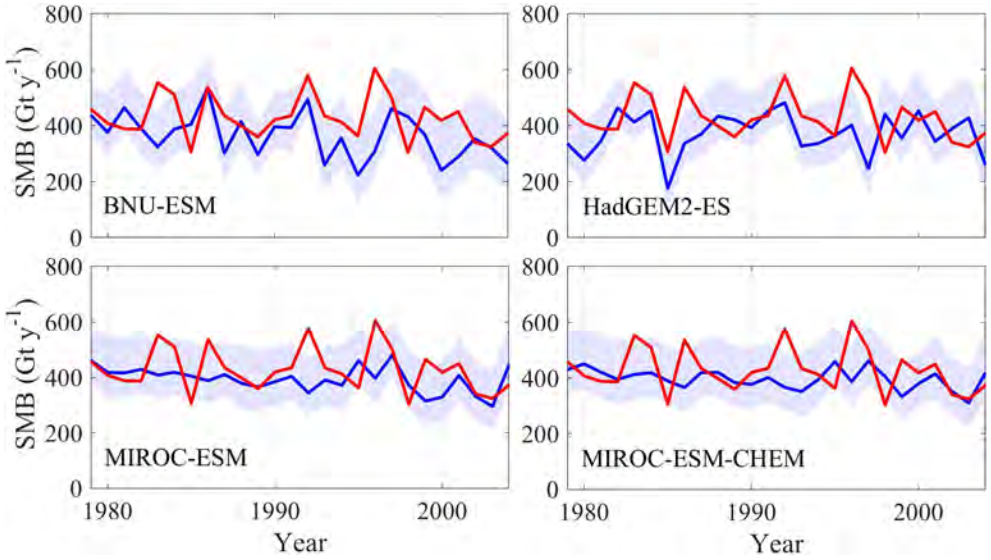

Figure 2. Time series of modeled surface mass balance using the SEMIC eight albedo parameterizations driven by the four models (blue curves and shadings showing multi-parameterization mean and the across-parameterization spread) and MAR (red curves).

surface elevation change due to ice flow is balanced by SMB. SMB anomalies relative to the historical averaged SMB will cause elevation change from 2006 onward. The product of cumulative SMB anomaly and SMB gradient gives the correction term for SMB.

3. Results

3.1. Surface Mass Balance

The multi-model mean near-surface air temperature under G4 is lower than that under RCP4.5 (and RCP8.5) over the whole 2020–2089 period (Figure 3 and Table 2). Greenland is 1.1 °C cooler under G4 than RCP4.5 during 2020–2069, while globally, the four ESMs show a reduction of 0.6 °C. There are large differences in the degree of relative cooling across the models, with the two MIROC models displaying a marked lack of cooling. The MIROC models also show very little over-cooling for Greenland relative to global means —only 0.1 °C compared with 0.3 °C for HadGEM2 and 1.4 °C for BNU-ESM (Table 2). This is consistent with the relatively small impact of SAI on the radiative fluxes in the MIROC models, especially the LW (Figure 3 and Table 2). Kashimura et al. (2017) show that changes in global mean SW fluxes in MIROC-ESM and MIROC-ESM-CHEM are the smallest among six ESMs they studied. However, even with the modest contribution from the MIROC models, there is an over-cooling of Greenland relative to the global mean, and especially relative to the other higher latitude areas which are generally under-cooled in G4. This suggests that factors unique to Greenland are operating.

Annual precipitation averages show increasing trends in all scenarios (Figure 3), but snowfall has no trends in any scenario. Precipitation and, to a smaller extent, snowfall are significantly lower under G4 than RCP4.5 (Table 2). Downward SW radiation at the surface shows decreasing trends over time due to increasing greenhouse gas emissions (Figure 3).

We calculate SMB (Figure 4) with the mass and energy balance model SEMIC (Krapp et al., 2017) driven by ½° × ½° downscaled data (Hempel et al., 2013). All models show that runoff under G4 is smaller than RCP4.5 and RCP8.5 (Figure S2). BNU-ESM and HadGEM2-ES decrease runoff and increase SMB more than MIROC-ESM and MIROC-ESM-CHEM, consistent with more cooling by those models (Table 2 and Figure 3), which is especially important during summer (Figure S3). The spatial distribution of multi-model mean SMB (2020–2069 and 2075–2089) under G4, RCP4.5, and RCP8.5 scenarios are very similar (Figure S4), with very high SMB gradients along the margins where surface elevation rapidly increases. Since the steep margins of the ice sheet are crucial in determining melt and overall SMB, we discuss only

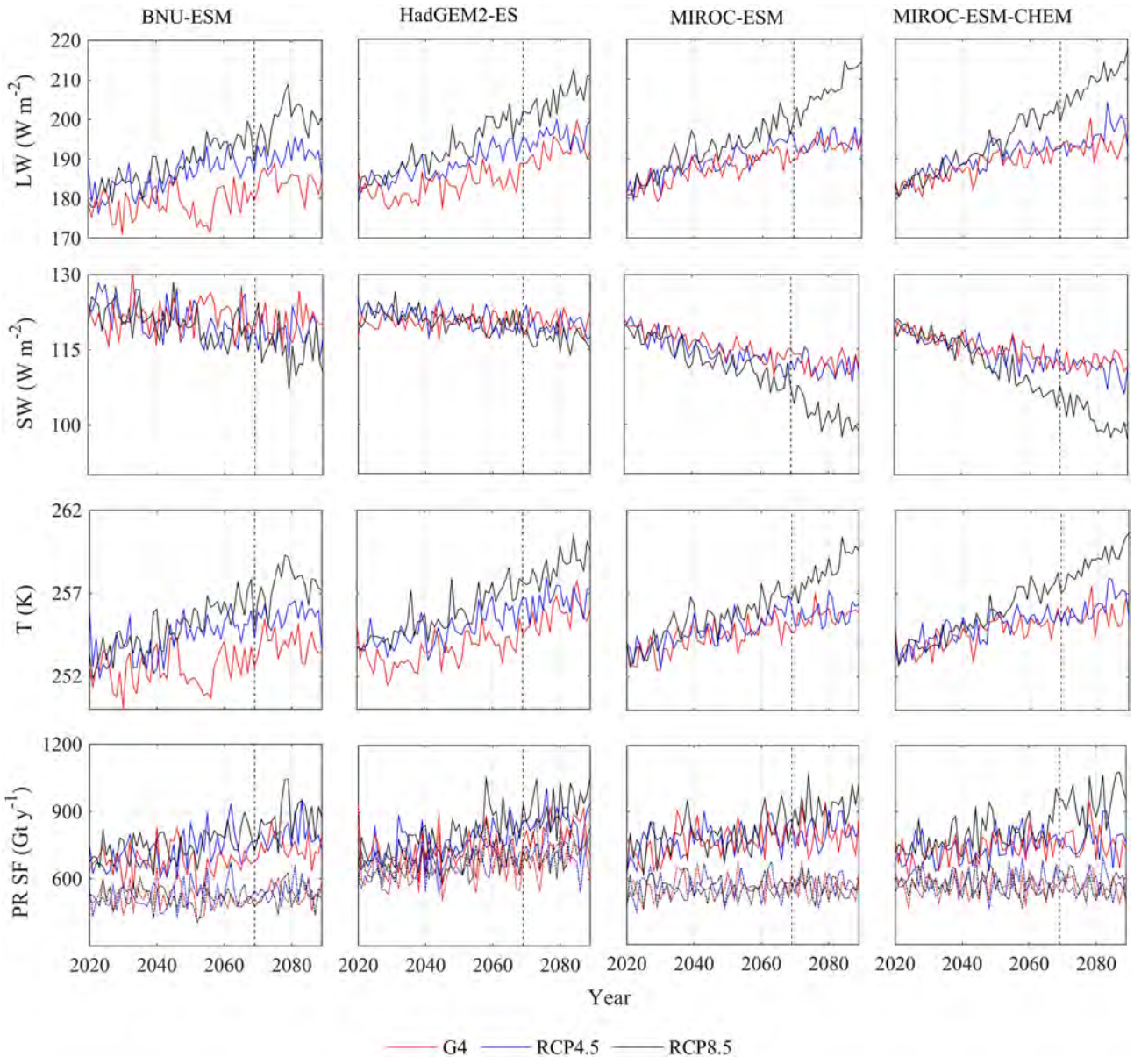

Figure 3. Annual downward longwave (LW) radiation, downward shortwave (SW) radiation, near-surface air temperature (T), precipitation (PR, solid curves), and snowfall (SF, dashed curves) for BNU-ESM (left column), HadGEM2-ES (second column), MIROC-ESM (third column), and MIROC-ESM-CHEM (right column) during 2020–2089 under G4, RCP4.5, and RCP8.5 scenarios over Greenland. Vertical dashed lines denote the end of the SAI.

Table 2
Differences (G4-RCP4.5) in Precipitation (PR), Snowfall (SF), Downward Shortwave (SW) Radiation, Downward Longwave (LW) Radiation, Specific Surface Humidity (q), and Near-Surface Air Temperature (T) Over the Greenland Ice Sheet and Over the Whole Earth During 2020–2069

Model	PR (mm year^{-1})	SF (mm year^{-1})	SW (W m^{-2})	LW (W m^{-2})	q (g kg^{-1})	Greenland T (°C)	Global T (°C)
BNU-ESM	**−16.9**	−5.8	**−0.2**	**−8.5**	**−0.102**	**−2.2**	**−0.8**
HadGEM2-ES	**−26.0**	−6.1	**−0.4**	**−5.6**	**−0.119**	**−1.4**	**−1.1**
MIROC-ESM	−11.2	1.3	**1.2**	**−2.3**	**−0.053**	**−0.5**	**−0.4**
MIROC-ESM-CHEM	−9.6	**−10.1**	**0.7**	**−1.9**	**−0.040**	**−0.4**	**−0.3**
Ensemble	**−15.9**	**−5.2**	**0.3**	**−4.6**	**−0.078**	**−1.1**	**−0.6**

Note. Entries in bold are significant at the 95% level according to the Wilcoxon signed-rank test.

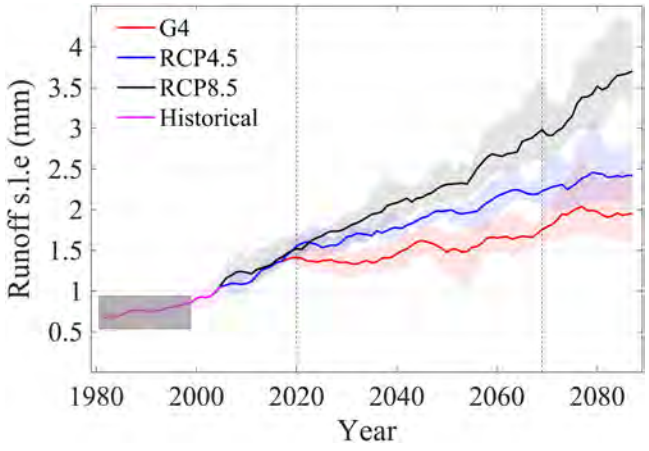

Figure 4. Time series (5-year moving average) of runoff (millimeters of sea level equivalent) from 1979 to 2089 calculated by SEMIC under RCP4.5, RCP8.5, and G4. The SEMIC results are the mean from eight albedo parameterizations driven by the four ESMs. The gray boxed region is from MAR driven by ERA-Interim over 1980–1999. Vertical dashed lines denote the beginning and end of the SAI. Colored shading indicates the across-model spread.

the results from SEMIC simulations driven by ½° downscaled climate forcing for the remainder of this article rather than the spatially much coarser ESM products. The multi-model ice sheet mean SMB and 95% confidence intervals ($N = 4$) from 2020 to the end of geoengineering in 2069 are 220 ± 50 Gt year^{-1} (G4), half that for RCP4.5 and close to zero (30 ± 85 Gt year^{-1}) for RCP8.5 (Table 3). G4 reduces runoff over the 50-year period by 20 ± 2% (the 95% confidence interval of the ensemble mean, $N = 200$; taking the across-model spread instead gives a confidence interval of 9–31%, $N = 4$) relative to RCP4.5 and 32 ± 2% (with across-model confidence interval of 22–42%) relative to RCP8.5.

G4 significantly reduces the temperature and downward LW radiation over the ice sheet relative to RCP4.5; however, downward SW radiation exhibits smaller and more variable changes (Figure 5 and Table 2). SMB under G4 is larger than that under RCP4.5 mainly over ice marginal ablation region and is governed by atmospheric water content (expressed as precipitation or specific humidity) along with temperature (Figures 5 and 6). This is perhaps surprising given expected reductions in SW forcing due to G4 of 0.5–1.5 W m^{-2} globally (Kashimura et al., 2017), but differences in SW forcing for high albedo surfaces such as the Greenland ice sheet must be small, and aerosol scattering is offset by reduced SW absorption by water vapor. SAI produces a weakened global hydrological cycle leading to lower precipitation (e.g., Fasullo et al., 2018; Huneeus et al., 2014; Irvine et al., 2010 , 2018; Kravitz et al., 2013) and humidity which reduces LW absorption. The dependence of SMB on temperature and moisture suggests (Figure 6) that a modified PDD approach could produce useful SMB estimates under SAI.

Much smaller changes occur in the accumulation region that comprises most of the ice sheet, where melting is very small and precipitation effects dominate. Analysis of SEMIC results showed significant trends between elevation and SMB only in the ablation zone in the southwest quadrant of the ice sheet, which is known to have the steepest gradients of mass balance with rising temperature (Pattyn et al., 2018), but even there the extra ablation amounts to only an extra 8–20 Gt year^{-1} in SMB (Figure S9) depending on scenario and ESM. This effect may be compared with inter-annual variability in SMB of typically 150 Gt (Figure S2). Hence, SMB-elevation feedback does not materially affect the analysis here, as was also previously concluded for cases of small temperature rises (Pattyn et al., 2018). These negligible topographic effects also imply that ice margin retreat has negligible impact on SMB estimates.

3.2. AMOC, Sea Ice, and Water Vapor

The observed AMOC as measured by the RAPID-MOCHA array (McCarthy et al., 2015) is rather variable on all timescales but has a mean over 2004–2012 of 17.2 ± 4.6 Sv. The ensemble mean of the four models is reasonably close to this (Figure 7b), but BNU-ESM is slightly too high and the MIROC pair of models rather too low. This suggests that the MIROC models are not capturing the process well, which may also contribute to their modest differences in Greenland SMB and smaller differences in temperatures between G4 and RCP4.5

Table 3
Modeled Surface Mass Balance (Gt year^{-1}) Using SEMIC Over Greenland During 2020–2069 and 2075–2089 Under G4, RCP4.5, and RCP8.5 Scenarios (With 95% Confidence Intervals, N = 4)

	G4		RCP4.5		RCP8.5	
Scenario/model	2020–2069	2075–2089	2020–2069	2075–2089	2020–2069	2075–2089
BNU-ESM	282	210	61	−42	−15	−344
HadGEM2-ES	229	48	74	−151	−70	−589
MIROC-ESM	210	80	164	75	83	−234
MIROC-ESM-CHEM	155	55	138	9	117	−283
Ensemble	219 ± 51	98 ± 74	109 ± 49	−27 ± 93	29 ± 85	−363 ± 154

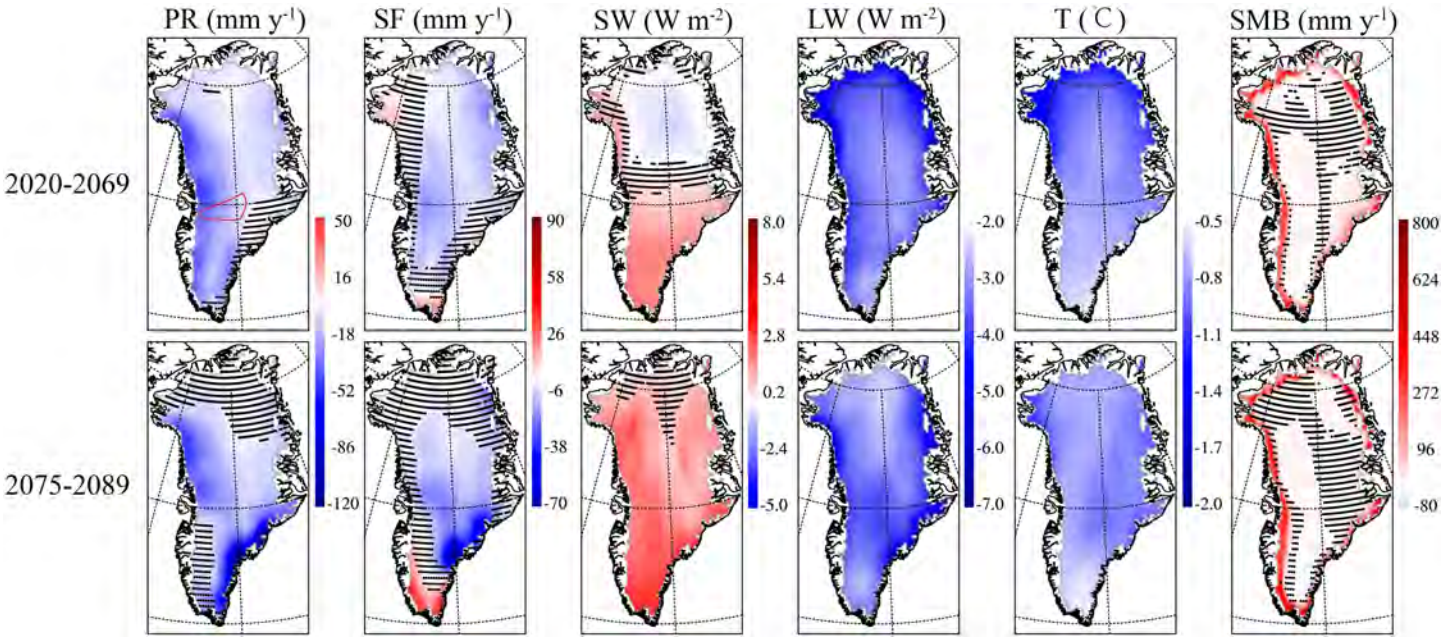

Figure 5. Maps of spatial differences (G4-RCP4.5) over Greenland of precipitation (PR), snowfall (SF), surface downward shortwave (SW) and longwave (LW) radiation fluxes, near-surface air temperature (T), and surface mass balance (SMB) during 2020–2069 and 2075–2089. Stippling indicates regions where differences are not significant at the 95% level according to the Wilcoxon signed-rank test. The Jakobshavn Isbrae drainage basin is outlined in red in the top left panel. Individual ESM results are shown in Figures S5–S8.

both globally and over Greenland (Table 2). Figure 7 shows that AMOC under G4 is stronger than under RCP4.5. AMOC response under G4 in all four ESMs is much closer to present-day conditions than under greenhouse gas forcing alone. A similar result was observed for seven ESMs that simulated the solar dimming G1 scenario (Hong et al., 2017) which, since it counters a quadrupling of CO_2 with reduced solar insolation, has a much larger signal/noise ratio than the SAI G4 experiment. However, in all geoengineering scenarios and for all the ESMs, the AMOC was somewhat reduced compared with the control. In contrast, the CESM running the GLENS SAI scenario (Fasullo et al., 2018) produces a stronger AMOC than present day, and much stronger than that under the RCP8.5 scenario.

AMOC under G4 increases heat flux from ocean to atmosphere relative to RCP4.5 (Figure 8e). But surface temperatures under G4 are cooler than RCP 4.5 (Figure 8a), which is consistent with a larger sea ice extent under G4 (Figure 8c). The combination of increased heat flux but cooler surface conditions is explained by the domination of surface radiation fluxes over AMOC in determining surface temperatures. Under G1 and G4, there is reduced air-sea temperature contrast and hence lower ocean-atmosphere heat exchange in the North Atlantic (Hong et al., 2017). Reduced heat loss from ocean to atmosphere suppresses evaporation and lowers the density of the northern North Atlantic, suppressing surface sinking under both greenhouse gas and geoengineered climates, and so slowing AMOC. Changes in wind and precipitation minus evaporation are much less important than those in radiative flux (Hong et al., 2017). The AMOC effectively warms the high latitude climate as it transfers heat from south to north. A weakened AMOC under greenhouse gas forcing tends to reduce high latitude surface warming, whereas a relatively less weakened AMOC under G1 and G4 geoengineering moderates the cooling effects. Hence, the impact on Greenland SMB from AMOC reduction could be expected to be a cooler surface, reducing mass loss.

Sea ice increases under G4 relative to RCP4.5 for all models, especially during the summer melt season as seen by the differences in September sea ice extent (Figures 7f and 8c). Increased ice cover fraction leads to reduced atmospheric moisture content and tends to be associated with reduced low level, water-bearing clouds (Figure 8d). However, the linkages between sea ice and atmospheric circulation in the Arctic are not simple, involving both barotropic and baroclinic flows which vary between regions and seasons (Moore et al., 2014; Rinke et al., 2019).

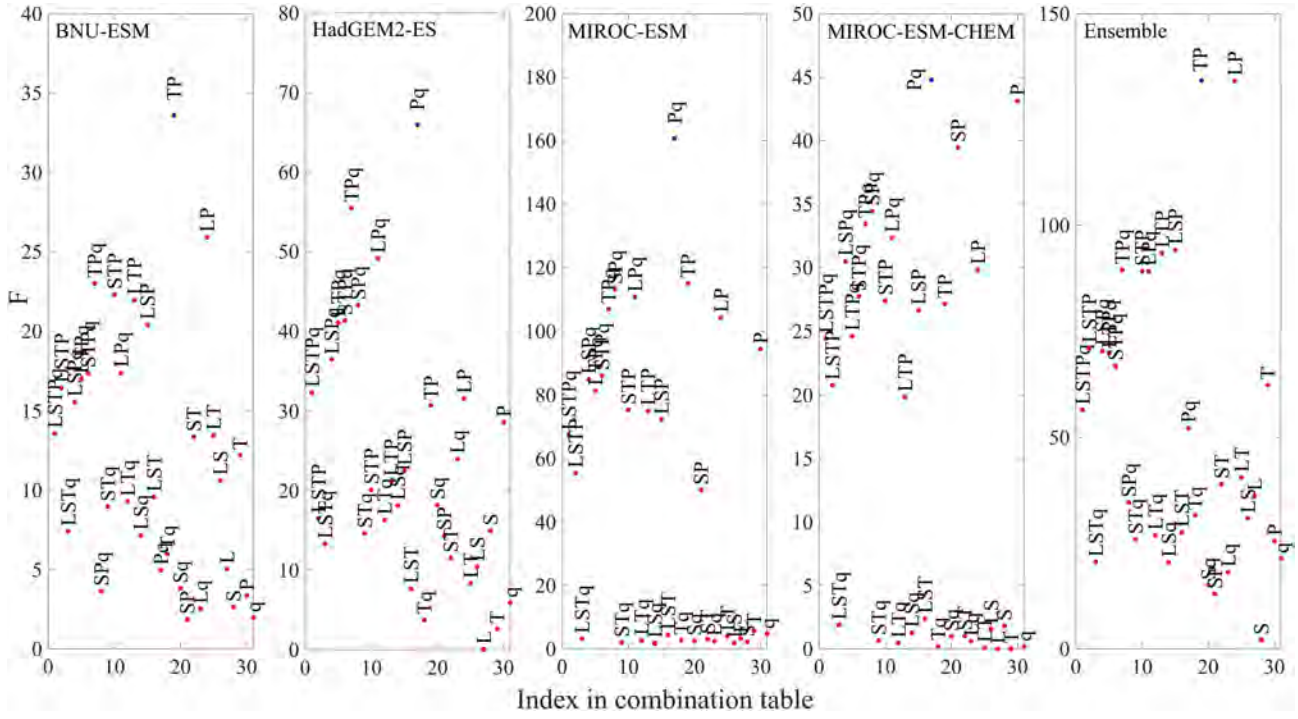

Figure 6. The *F* statistic of the 31 different combinations of regression variables for SMB differences between G4 and RCP4.5 for each ESM separately as labeled and the four-model ensemble. The *x* axis on each panel represents the combination of components used as predictors in each regression equation $SMB_{G4\text{-}RCP4.5} = \sum_{i=1}^{5} (M_i X_i)$ where $X = \{T,P,L,S,q\}$ representing surface temperature, precipitation, downward longwave radiation, downward shortwave radiation, and specific surface humidity, respectively. The best fitting model for each ESM is marked by a blue symbol.

Low elevation water-bearing clouds have dramatic effects on Greenland surface melt, refreezing, and net runoff from the ice sheet (Van Tricht et al., 2016). The low elevation margins are the places where most melt occurs and which are most affected by proximate changes across the Arctic waters. Low clouds are

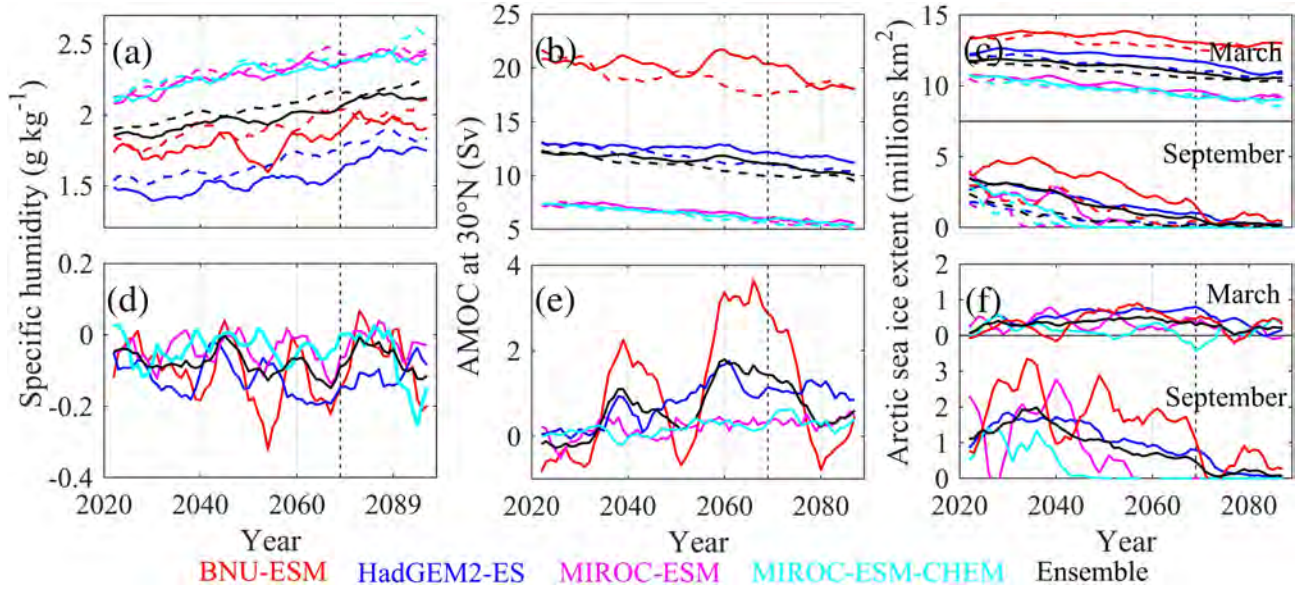

Figure 7. Five-year moving averages of forcing fields. (a) Annual mean surface specific humidity, (b) AMOC index defined as the annual mean maximum volume transport streamfunction at 30° in the North Atlantic, and (c) Arctic sea ice extent (defined at limit of 15% ice concentration region) from four ESMs during 2020–2089 under G4 and RCP4.5 scenarios. Solid curves are G4 and dashed RCP4.5 results. Panels (d) to (f) show differences G4-RCP4.5. Vertical dashed line marks the end of SAI at 2069.

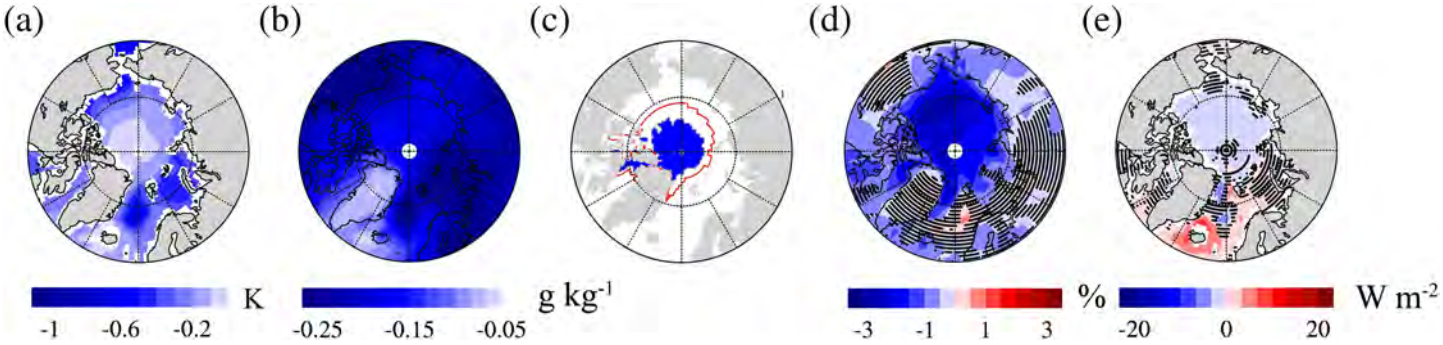

Figure 8. Ensemble mean differences (G4-RCP4.5) over 2020–2069 over the Arctic. (a) Sea surface temperature, (b) surface specific humidity, and (c) September sea ice extent; red line is G4, blue is RCP4.5. (d) Low cloud and (e) heat flux from ocean to atmosphere; stippling indicates regions where differences are not significant at the 95% level according to the Wilcoxon signed-rank test. Panels (a) to (c) are for four-model ensemble: BNU-ESM, MIROC-ESM, MIROC-ESM-CHEM, and HadGEM2-ESM. Panels (d) and (e) for only first three models. Individual model results are in Figures S10–S14.

significantly reduced over the Arctic, but for Greenland the reduction is modest (Figure 8d), and furthermore, clouds are notoriously difficult to parameterize in ESM (Schneider et al., 2017). However, surface humidity is highly correlated with LW radiation both in observations (Ruckstuhl et al., 2007) and in the ESM used here (Figure S15). Surface humidity over Greenland (Figure 8b) is 4% lower (range across four ESMs: 2–6%; Figure 7a) under G4 accounting for about 3.4 W m^{-2} (Figure S15) or 74% (ranging from 41% for BNU-ESM to 81% for HadGEM2-ES) of the G4-RCP4.5 difference (Table 2). This means that the ablation regions are affected by both the globally reduced strength of the hydrological cycle under SAI (Kravitz et al., 2013) and the increased sea ice cover reducing local atmospheric water supply. Reduced runoff under G4 relative to RCP4.5 is consistent with increases in local summer sea ice cover, cooler surface waters, and reduced evaporation, despite AMOC changes tending to transport somewhat more ocean heat toward Greenland than under greenhouse forcing alone. SW forcing by clouds has also been evoked to explain change in Greenland SMB (Hofer et al., 2017) and that these changes are related to variations in the North Atlantic Oscillation. For the 20 years after terminating SAI, downward SW radiation is larger than under RCP4.5 across most of ice sheet, consistent with cooler temperatures leading to reduced humidity and decreased radiative absorption at both SW and LW. The decadal-scale duration suggests sea ice or oceanic drivers rather than atmospheric ones.

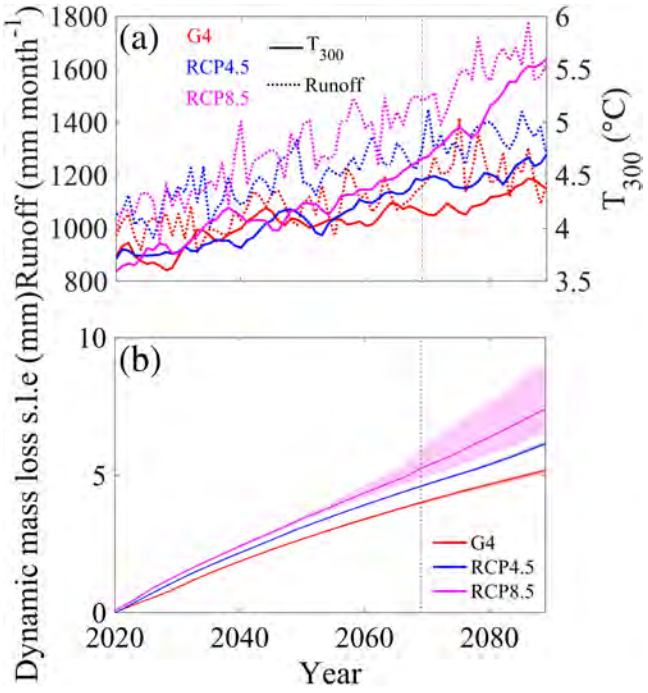

Figure 9. Jakobshavn Isbrae mass loss due to grounding line retreat and dynamic thinning. (a) Four-ESM ensemble mean climate forcing for Jakobshavn Isbrae under the RCP8.5, RCP4.5, and G4 scenarios: 300-m depth ocean temperatures near the mouth of Ilulissat fjord (solid) and annual maximum monthly surface water runoff near the glacier terminus given by SEMIC (dotted). (b) The ensemble mean global sea level contribution (sold lines) and four-ESM spread (shaded) from BISICLES simulations.

3.3. Ice Dynamics

The calving of ice bergs into the ocean accounts for about 50% of ice loss from Greenland (van den Broeke et al., 2009). The terminus of just five dynamically thinning glaciers in Greenland, amounting less than 1% of Greenland's area, contributed more than 12% of the net ice loss in recent years (McMillan et al., 2016). Ocean temperatures have been shown to explain much of the recent retreat and inter-annular variability in terminus position of outlet glaciers (Bondzio et al., 2018; Cowton et al., 2018). We estimate the potential impact of SAI on dynamical process by considering the three-dimensional BISICLES ice dynamics model (Guo et al., 2019) of Jakobshavn Isbrae (Figure 5), the fastest and largest individual contributor of Greenland's outlets to recent sea level rise (McMillan et al., 2016). The model has parameterizations to represent the effects of ice mélange buttressing, crevasse-depth-based calving, and submarine melting and reproduces well the glacier's recent evolution (Guo et al., 2019). We find (Figure 9) that dynamic ice losses are 15 ± 1% (95% confidence interval, $N = 200$) lower under G4 than under RCP4.5 by 2070. Figure 9 shows that both ocean temperatures and surface runoff change

much less under RCP4.5 and G4 than under RCP8.5 over the 21st century and is reflected in their simulated mass losses. The modest differences in 300-m ocean temperatures and mass loss between G4 and RCP4.5 are consistent with the observed forcing by ocean temperatures of Greenland outlets (Cowton et al., 2018).

The ocean warming in front of Jakobshavn Isbrae reflects the general warming of the North Atlantic although the spread of warming waters around Greenland will certainly be spatially variable. This means that it is plausible to expect a statistically similar scaling of dynamical response at other glaciers, despite their internal dynamical variability and local bathymetric effects. The impact of SAI on the dynamical response is less than it is on the SMB. This is due to the domination of Greenland ice dynamics by ocean forcing, which warms relatively slowly because of the AMOC changes discussed earlier.

4. Conclusions

Our analysis of four ESMs reveals fairly large differences in implied changes to Greenland SMB (Table 3). In particular, the two MIROC models show relatively small changes in surface temperatures, radiative fluxes, and AMOC under G4 compared with RCP4.5 (Table 2). Observed AMOC is also significantly stronger than simulated by the MIROC models. These deficiencies lead to relatively small over-cooling over Greenland in the MIROC models (Table 2). As we discuss in section 2.1, the two MIROC models share several common features and are not therefore as independent as the other two models we use. Despite this, even moderate de-weighting (0.75 each) of the MIROC raises the runoff results by only a few percent, but altogether removing the MIROC models increases the changes in runoff under G4 relative to RCP4.5 from about 20% to 29%. Perhaps a bigger problem with the utility of the G4 scenario is that it is quite simplistic—just assuming a constant equatorial injection into the lower stratosphere does not allow for the detailed control of the important pole-equator gradients that are probably very important to maintaining fundamental circulation patterns such as the Hadley circulation (Davis et al., 2016; Guo et al., 2018). Equatorial-only SAI leads to under-cooling of the high latitudes relative to tropics (Kravitz et al., 2013), and SAI without this spatial pattern, such as produced by the GLENS simulations (Tilmes et al., 2018), might well produce more benefits for Greenland ice sheet mass conservation for the same amount of aerosol injected. The GLENS simulations have only been published for a single ESM to date because the feedback-control adjustments demand extensive analysis of each ESM (Kravitz et al., 2016), but such simulations will surely be more true to life of any actual deployment of SAI in future and so should be a research priority.

The 15% reduction in the half of present-day total mass loss due to dynamic changes, added to the 20% reduction in the half due to surface runoff, means that total sea level rise from Greenland by 2070 under G4 would be 17.5%, lower than under the RCP4.5 scenario. The presently unquantifiable uncertainty in extending this result to total dynamic losses leads us to suggest a 15–20% lower sea level rise for G4 than RCP4.5. This is less than the 30% reduction in sea level rise from the High Mountain Asia glaciers (Zhao et al., 2017) under G4 relative to RCP4.5, mainly due to the unique response of the North Atlantic and AMOC. Sea ice, AMOC, and cloud cover return to values essentially the same as RCP4.5 within 5–10 years following termination of SAI in 2016 (Figure 7), but both runoff (Figure 4), and especially dynamical ice losses (Figure 9) remain well below RCP4.5 levels until at least 2089. This is a long-lasting effect of preserving the ice sheet during the SAI period.

The fast-flowing Greenland glaciers mainly flow into narrow, deeply incised fjords and are potentially amenable to targeted engineering approaches to restrict warm water access to their floating tongues (Hunt & Byers, 2019; Moore et al., 2018; Wolovick & Moore, 2018). However, this localized approach to slowing ice dynamical ice loss would likely be ineffective in isolation if surface temperatures continued to rise because surface melt would lead to hydro-fracture and the disintegration of any floating parts of glaciers. This means that preventing air temperatures rising, either through aggressive greenhouse gas mitigation or through geoengineering, would also be needed to maintain the ice sheet close to its present form. The Greenland ice sheet is expected lose at least 90% of its current volume if ice sheet summer temperatures warm by around a 1.8 °C above pre-industrial (Pattyn et al., 2018). Temperatures above this, would in the long term, lead to multi-meter sea level rise commitments. Under G4 SAI summer temperatures rises are 1.6 °C, so likely below this threshold—although large uncertainties remain in the way the ESMs treat stratospheric aerosol physics and chemistry (MacMartin & Kravitz, 2019).

Regardless of long-term sea level rise, the 15–20% reduction in mass loss from the ice sheet under G4 compared with RCP4.5 this century endorses the view (MacMartin & Kravitz, 2019): SAI geoengineering is worth serious consideration, both of the desirable effects and of potential unwanted side effects, in far more detail than to date.

Acknowledgments
We thank all participants of the GeoMIP and their model development teams in particular Andy Jones for running the HadGEM2-ES GeoMIP simulations that are analyzed here; the CLIVAR/WCRP Working Group on Coupled Modeling for endorsing the GeoMIP; and the scientists managing the Earth System Grid (ESG) data nodes who have assisted with making GeoMIP output available. ESM data are available from the ESG, and downscaled data can be produced following Hempel et al. (2013) and using SEMIC (Krapp et al., 2017). The authors will assist if necessary. The authors have no competing interests.

References

Applegate, P. J., & Keller, K. (2015). How effective is albedo modification (solar radiation management geoengineering) in preventing sea-level rise from the Greenland Ice Sheet? *Environmental Research Letters*, *10*(8), 84018. https://doi.org/10.1088/1748-9326/10/8/084018

Beven, K. J., & Kirby, M. J. (1979). A physically based, variable contributing area model of basin hydrology. *Hydrological Sciences Bulletin*, *24*(1), 43–69. https://doi.org/10.1080/02626667909491834

Bluth, G. J. S., Doiron, S. D., Schnetzler, C. C., Krueger, A. J., & Walter, L. S. (1992). Global tracking of the SO_2 clouds from the June 1991 Mount Pinatubo eruptions. *Geophysical Research Letters*, *19*, 151–154.

Bondzio, J. H., Morlighem, M., Seroussi, H., Wood, M. H., & Mouginot, J. (2018). Control of ocean temperature on Jakobshavn Isbræ's present and future mass loss. *Geophysical Research Letters*, *45*, 12–912.

Braithwaite, R. J. (1995). Positive degree-day factors for ablation on the Greenland ice sheet studied by energy-balance modelling. *Journal of Glaciology*, *41*, 153–160.

van den Broeke, M., van den Broeke, M., Bamber, J. L., Ettema, J., Rignot, E., Schrama, E., et al. (2009). Partitioning recent Greenland mass loss. *Science*, *326*, 984–986.

Collins, W. J., Bellouin, N., Doutriaux-Boucher, M., Gedney, N., Halloran, P., Hinton, T., et al. (2011). Development and evaluation of an Earth-System model—HadGEM2. *Geoscientific Model Development*, *4*, 1051–1075. https://doi.org/10.5194/gmd-4-1051-2011

Cowton, T. R., Sole, A. J., Nienow, P. W., Slater, D. A., & Christoffersen, P. (2018). Linear response of east Greenland's tidewater glaciers to ocean/atmosphere warming. *Proceedings of the National Academy of Sciences of the United States of America*, *115*(31), 7907–7912. https://doi.org/10.1073/pnas.1801769115

Dai, Y., Zeng, X., Dickinson, R. E., Baker, I., Bonan, G. B., Bosilovich, M. G., et al. (2003). The common land model (CLM). *Bulletin of the American Meteorological Society*, *84*, 1013–1023. https://doi.org/10.1175/BAMS-84-8-1013

Davis, N. A., Seidel, D. J., Birner, T., Davis, S. M., & Tilmes, S. (2016). Changes in the width of the tropical belt due to simple radiative forcing changes in the GeoMIP simulations. *Atmospheric Chemistry and Physics*, *16*, 10083–10095. https://doi.org/10.5194/acp-16-10083-2016

Ettema, J. (2009). Higher surface mass balance of the Greenland ice sheet revealed by high-resolution climate modeling. *Geophysical Research Letters*, *36*, L12501. https://doi.org/10.1029/2009GL038110

Fasullo, J. T., Tilmes, S., Richter, J. H., Kravitz, B., MacMartin, D. G., Mills, M. J., & Simpson, I. R. (2018). Persistent polar ocean warming in a strategically geoengineered climate. *Nature Geoscience*, *11*(12), 910–914. https://doi.org/10.1038/s41561-018-0249-7

Fettweis, X., Franco, B., Tedesco, M., van Angelen, J. H., Lenaerts, J. T. M., van den Broeke, M. R., & Gallée, H. (2013). Estimating the Greenland ice sheet surface mass balance contribution to future sea level rise using the regional atmospheric climate model MAR. *The Cryosphere*, *7*, 469–489. https://doi.org/10.5194/tc-7-469-2013

Guo, A., Moore, J. C., & Ji, D. (2018). Tropical atmospheric circulation response to the G1 sunshade geoengineering radiative forcing experiment. *Atmospheric Chemistry and Physics*, *18*, 8689–8706. https://doi.org/10.5194/acp-18-8689-2018

Guo, X., Zhao, L., Gladstone, R., Sun, S., & Moore, J. C. (2019). Simulated retreat of Jakobshavn Isbræ during the 21st century. *The Cryosphere* accepted, *13*(11), 3139–3153.

Hanna, E., Navarro, F. J., Pattyn, F., Domingues, C. M., Fettweis, X., Ivins, E. R., et al. (2013). Ice-sheet mass balance and climate change. *Nature*, *498*(7452), 51–59. https://doi.org/10.1038/nature12238

Hempel, S., Frieler, K., Warszawski, L., Schewe, J., & Piontek, F. (2013). A trend-preserving bias correction—The ISI-MIP approach. *Earth System Dynamics*, *4*, 219–236.

Hofer, S., Tedstone, A. J., Fettweis, X., & Bamber, J. L. (2017). Decreasing cloud cover drives the recent mass loss on the Greenland Ice Sheet. *Science Advances*, *3*, e1700584.

Hong, Y., Moore, J. C., Jevrejeva, S., Ji, D., Phipps, S., Lenton, A., et al. (2017). Impact of the GeoMIP G1 sunshade geoengineering experiment on the Atlantic Meridional Overturning Circulation. *Environmental Research Letters*, *12*(3), 034009. https://doi.org/10.1088/1748-9326/aa5fb8

Huneeus, N., Boucher, O., Alterskjær, K., Cole, J. N. S., Curry, C. L., Ji, D., et al. (2014). Forcings and feedbacks in the GeoMIP ensemble for a reduction in solar irradiance and increase in CO2. *Journal of Geophysical Research: Atmospheres*, *119*, 5226–5239. https://doi.org/10.1002/2013JD021110

Hunt, J. D., & Byers, E. (2019). Reducing sea level rise with submerged barriers and dams in Greenland. *Mitigation and Adaptation Strategies for Global Change*, *24*, 779–794.

Irvine, P. J., Keith, D. W., & Moore, J. C. (2018). Brief communication: Understanding solar geoengineering's potential to limit sea level rise requires attention from cryosphere experts. *The Cryosphere*, *12*, 2501–2513.

Irvine, P. J., Ridgwell, A., & Lunt, D. J. (2010). Assessing the regional disparities in geoengineering impacts. *Geophysical Research Letters*, *37*, L18702. https://doi.org/10.1029/2010GL044447.13

Jevrejeva, S., Jackson, L. P., Riva, R. E. M., Grinsted, A., & Moore, J. C. (2016). Coastal sea level rise with warming above 2 °C. *Proceedings of the National Academy of Sciences of the United States of America*, *113*(47), 13,342–13,347. https://doi.org/10.1073/pnas.1605312113

Ji, D., Wang, L., Feng, J., Wu, Q., Cheng, H., Zhang, Q., et al. (2014). Description and basic evaluation of Beijing Normal University Earth System Model (BNU-ESM) version 1. *Geoscientific Model Development*, *7*, 2039–2064. https://doi.org/10.5194/gmd-7-2039-2014

Jones, A. C., Hawcroft, M. K., Haywood, J. M., Jones, A., Guo, X., & Moore, J. C. (2018). Regional climate impacts of stabilizing global warming at 1.5 K using solar geoengineering. *Earth's Future*, *6*(2), 230–251. https://doi.org/10.1002/2017EF000720

Kashimura, H., Abe, M., Watanabe, S., Sekiya, T., Ji, D., Moore, J. C., et al. (2017). Shortwave radiative forcing, rapid adjustment, and feedback to the surface by sulfate geoengineering: Analysis of the Geoengineering Model Intercomparison Project G4 scenario. *Atmospheric Chemistry and Physics*, *17*, 3339–3356. https://doi.org/10.5194/acp-17-3339-2017

Kitous, A., & Keramidas, K. (2015). Analysis of scenarios integrating the INDCs. *European Commission*.

Krapp, M., Robinson, A., & Ganopolski, A. (2017). SEMIC: An efficient surface energy and mass balance model applied to the Greenland ice sheet. *The Cryosphere*, *11*, 1519–1535.

Kravitz, B., Caldeira, K., Boucher, O., Robock, A., Rasch, P. J., Alterskjær, K., et al. (2013). Climate model response from the geoengineering model intercomparison project (GeoMIP). *Journal of Geophysical Research: Atmospheres*, *118*, 8320–8332. https://doi.org/10.1002/jgrd.50646
Kravitz, B., MacMartin, D. G., Wang, H., & Rasch, P. J. (2016). Geoengineering as a design problem. *Earth System Dynamics*, *7*, 469–497. https://doi.org/10.5194/esd-7-469-2016
Kravitz, B., Robock, A., Boucher, O., Schmidt, H., Taylor, K. E., Stenchikov, G., & Schulz, M. (2011). The geoengineering model intercomparison project (GeoMIP). *Atmospheric Science Letters*, *12*(2), 162–167.
MacMartin, D. G., & Kravitz, B. (2019). Mission-driven research for stratospheric aerosol geoengineering. *Proceedings of the National Academy of Sciences of the United States of America*, *116*, 1089–1094.
McCarthy, G. D., Smeed, D. A., Johns, W. E., Frajka-Williams, E., Moat, B. I., Rayner, D., et al. (2015). Measuring the Atlantic meridional overturning circulation at 26°N. *Progress in Oceanography*, *130*, 91–111. https://doi.org/10.1016/j.pocean.2014.10.006
McMillan, M., Leeson, A. A., Shepherd, A., Briggs, K., Armitage, T., Hogg, A., et al. (2016). A high resolution record of Greenland mass imbalance. *Geophysical Research Letters*, *43*, 7002–7010. https://doi.org/10.1002/2016GL069666
Moore, J. C., Gladstone, R., Zwinger, T., & Wolovick, M. (2018). Geoengineer polar glaciers to slow sea-level rise. *Nature*, *555*, 303–305.
Moore, J. C., Rinke, A., Yu, X., Ji, D., Cui, X., Li, Y., et al. (2014). Arctic sea ice and atmospheric circulation under the GeoMIP G1 scenario. *Journal of Geophysical Research: Atmospheres*, *119*, 567–583. https://doi.org/10.1002/2013JD021060
Morlighem, M., Williams, C. N., Rignot, E., An, L., Arndt, J. E., Bamber, J. L., et al. (2017). BedMachine v3: Complete bed topography and ocean bathymetry mapping of Greenland from multibeam echo sounding combined with mass conservation. *Geophysical Research Letters*, *44*, 11,051–11,061. https://doi.org/10.1002/2017GL074954
Noël, B., van de Berg, W. J., Machguth, H., Lhermitte, S., Howat, I., Fettweis, X., & van den Broeke, M. R. (2016). A daily, 1 km resolution data set of downscaled Greenland ice sheet surface mass balance (1958–2015). *The Cryosphere*, *10*, 2361–2377. https://doi.org/10.5194/tc-10-2361-2016
Pattyn, F., Ritz, C., Hanna, E., Asay-Davis, X., DeConto, R., Durand, G., et al. (2018). The Greenland and Antarctic ice sheets under 1.5 °C global warming. *Nature Climate Change*, *8*(12), 1053–1061. https://doi.org/10.1038/s41558-018-0305-8
Rignot, E., Box, J. E., Burgess, E., & Hanna, E. (2008). Mass balance of the Greenland ice sheet from 1958 to 2007. *Geophysical Research Letters*, *35*, L20502. https://doi.org/10.1029/2008GL035417
Rinke, A., Knudsen, E. M., Mewes, D., Dorn, W., Handorf, D., Dethloff, K., & Moore, J. C. (2019). Arctic summer sea ice melt and related atmospheric conditions in coupled regional climate model simulations and observations. *Journal of Geophysical Research: Atmospheres*, *124*, 6027–6039. https://doi.org/10.1029/2018JD030207
Ruckstuhl, C., Philipona, R., Morland, J., & Ohmura, A. (2007). Observed relationship between surface specific humidity, integrated water vapor, and longwave downward radiation at different altitudes. *Journal of Geophysical Research Atmospheres*, *112*, D03302. https://doi.org/10.1029/2006JD007850
Schneider, T., Teixeira, J., Bretherton, C. S., Brient, F., Pressel, K., Schär, C., & Siebesma, A. (2017). Climate goals and computing the future of clouds. *Nature Climate Change*, *7*, 3–5.
Simmons, A. (2006). ERA-Interim: New ECMWF reanalysis products from 1989 onwards. *ECMWF Newsletter*, *110*, 25–36.
Stroeve, J. (2001). Assessment of Greenland albedo variability from the advanced very high resolution radiometer Polar Pathfinder data set. *Journal of Geophysical Research*, *106*, 33,989–34,006.
Takata, K., Emori, S., & Watanabe, T. (2003). Development of the minimal advanced treatments of surface interaction and runoff. *Global and Planetary Change*, *38*, 209–222.
Taylor, K. E., Stouffer, R. J., & Meehl, G. A. (2012). An overview of CMIP5 and the experiment design. *Bulletin of the American Meteorological Society*, *93*, 485–498.
Tilmes, S., Richter, J. H., Kravitz, B., MacMartin, D. G., Mills, M. J., Simpson, I. R., et al. (2018). CESM1(WACCM) stratospheric aerosol geoengineering large ensemble project. *Bulletin of the American Meteorological Society*, *99*(11), 2361–2371. https://doi.org/10.1175/BAMS-D-17-0267.1
Van de Berg, W. J., Van Den Broeke, M., Ettema, J., Van Meijgaard, E., & Kaspar, F. (2011). Significant contribution of insolation to Eemian melting of the Greenland ice sheet. *Nature Geoscience*, *4*(10), 679–683. https://doi.org/10.1038/NGEO1245
Van Tricht, K., Lhermitte, S., Lenaerts, J., Gorodetskaya, I., L'Ecuyer, T., Noël, B., et al. (2016). Clouds enhance Greenland ice sheet meltwater runoff. *Nature Communications*, *7*(1), 10266. https://doi.org/10.1038/ncomms10266
Watanabe, S., Hajima, T., Sudo, K., Nagashima, T., Takemura, T., Okajima, H., et al. (2011). MIROC-ESM 2010: Model description and basic results of CMIP5-20c3m experiments. *Geoscientific Model Development*, *4*, 845–872. https://doi.org/10.5194/gmd-4-845-2011
Wolovick, M. J., & Moore, J. C. (2018). Stopping the flood: Could we use targeted geoengineering to mitigate sea level rise? *The Cryosphere*, *12*, 2955–2967.
Yang, D., Kane, D., Zhang, Z., Legates, D., & Goodison, B. (2005). Bias corrections of long-term (1973–2004) daily precipitation data over the northern regions. *Geophysical Research Letters*, *32*, L19501. https://doi.org/10.1029/2005GL024057
Zhao, L., Yang, Y., Cheng, W., Ji, D., & Moore, J. C. (2017). Glacier evolution in high-mountain Asia under stratospheric sulfate aerosol injection geoengineering. *Atmospheric Chemistry and Physics*, *17*, 6547–6564.

References From the Supporting Information

Baker, G., Ruschy, D., & Wall, D. (1990). The albedo decay of prairie snows. *Journal of Applied Meteorology*, *29*, 179–187.
Denby, B., Greuell, W., & Oerlemans, J. (2002). Simulating the Greenland atmospheric boundary layer Part I: Model description and validation. *Tellus*, *54*, 512–528.
Douville, H., Royer, J. F., & Mahfouf, J. (1995). A new snow parameterization for the Meteo-France climate model. *Climate Dynamics*, *12*, 21–35.
IAHS/UNESCO (1998). *Fluctuations of glaciers 1990–1995* (Vol. VII). Zurich: World Glacier Monitoring Service.
Serreze, M., Holland, M., & Stroeve, J. (2007). Perspectives on the Arctic's shrinking ice cover. *Science*, *315*(5818), 1533–1536. https://doi.org/10.1126/science.1139426
Slater, A. G., Pitman, A. J., & Desborough, C. E. (1998). The validation of a snow parameterization designed for use in general circulation models. *International Journal of Climatology*, *18*, 595–617.
Verseghy, D. L. (1991). CLASS—A Canadian Land Surface Scheme for GCMS.1. Soil model. *International Journal of Climatology*, *11*, 111–133.